Renewable Energy xxx (2017) 1–11

Contents lists available at ScienceDirect

Renewable Energy

journal homepage: www.elsevier.com/locate/renene

Simulating current-energy converters: SNL-EFDC model development, verification, and parameter estimation

Scott C. James [a, *], Erick L. Johnson [b], Janet Barco [c], Jesse D. Roberts [d]

[a] Baylor University, Departments of Geosciences & Mechanical Engineering, One Bear Place #97354, Waco, TX, USA
[b] Montana State University, Department of Mechanical & Industrial Engineering, 220 Roberts Hall, PO Box 173800, Bozeman, MT, USA
[c] Facultad de Ingeniería, Universidad de Medellín, Carrera 87 N° 30-65, Medellín, Colombia
[d] Sandia National Laboratories, Water Power Technologies Department, 1515 Eubank SE, MS 1124, Albuquerque, NM, USA

ARTICLE INFO

Article history:
Received 30 September 2016
Received in revised form
30 June 2017
Accepted 3 July 2017
Available online xxx

Keywords:
Marine renewable energy
Current-energy conversion
Numerical modeling
SNL-EFDC

ABSTRACT

Increasing interest in power production from ocean, tidal, and river currents has led to significant efforts to maximize energy conversion through optimal design and siting and to minimize effects on the environment. Turbine-based, current-energy-converter (CEC) technologies remove energy from current-driven systems and in the process generate distinct wakes, which can interact with other CEC devices and can alter flow regimes, sediment dynamics, and water quality. This work introduces Sandia National Laboratories-Environmental Fluid Dynamics Code CEC module and verifies it against a two-dimensional analytical solution for power generation and hydrodynamic response of flow through a CEC tidal fence. With a two-dimensional model that accurately reflects an analytical solution, the effort was extended to three-dimensional models of three different laboratory-flume experiments that measured the impacts of CEC devices on flow. Both flow and turbulence model parameters were then calibrated against wake characteristics and turbulence measurements. This is the first time that turbulence parameter values have been specified for CEC devices. Measurements and simulations compare favorably and demonstrate the utility and accuracy of this numerical approach for simulating the impacts of CEC devices on the flow field. The model can be extended to future siting and analyses of CEC arrays in complex domains.

1. Introduction

Current-energy converters (CECs) are a family of marine renewable-energy devices that harvest electrical power from water currents, such as those in river and tidal systems, to generate electricity. These devices hold promise as a non-consumable, domestic energy source; however, research is needed to make their cost of electricity competitive with other energy sources and to understand commensurate hydrodynamic and environmental effects [1]. System changes will be site-specific, necessitating an approach that can simulate various CEC technologies placed within any relevant marine or riverine system to predictively assess both hydrodynamic and environmental changes. Such an approach would be able to address questions about individual deployments and inform the decisions of regulatory agencies, opinions of stakeholder groups, and commitments from energy-project developers and investors [2].

While deploying a single test device is unlikely to significantly alter the flow and environment in any significant way, commercial arrays must be analyzed to ensure environmental thresholds are not exceeded. An analytical solution has been derived for a tidal strait that indicates a limit to the number of CEC devices that can be added to a system before the commensurate flow reduction yields less total energy generated [3,4]. At this transition point, the flow rate has been reduced by over 40%. More detailed modeling tools are required to investigate wake persistence and turbulent loadings from upstream devices that may necessitate broader array spacing to maximize performance and reliability. Hasegawa, Sheng, Greenberg and Thompson [5] performed a modeling study of the potential impact of CEC arrays on the Bay of Fundy and Gulf of Maine, which demonstrated that effects were not restricted to the immediate vicinity of the array. Tidal elevations were altered up to a few percent along a large portion of the coast outside of the Gulf. Due to the unique wetting and drying cycle of near-shore shallows,

* Corresponding author.
E-mail address: SC_James@baylor.edu (S.C. James).

http://dx.doi.org/10.1016/j.renene.2017.07.020
0960-1481/

the health of adjacent wetlands could be impacted [6]. The flow, sediment-dynamics, and water-quality simulator, Delft3D [7], has been used to model energy extraction from tidal flows [8–10]. Changes in bed shear and turbulence alter sediment dynamics affecting erosion/deposition regions [11–14]. A 2-D hydro-environmental model DIVAST was used to study the coastal environment and velocities adjacent to a 2000-device CEC array [15]. While water levels were largely unchanged, there was an increase in suspended sediment and fecal bacteria within 15 km of the array. Through each of these investigations it is obvious that altering the water circulation patterns impacts flushing rates, affecting algae-growth patterns and concentrations of nutrients and dissolved gases [16]. As none of these models represent a planned deployment, they provide a unique opportunity to investigate thresholds for array sizes and locations and their impact upon the environment. In addition, acoustic energy and electromagnetic waves emanating from CEC devices, and associated infrastructure, may further perturb wildlife behavior [2,17–20], but are not presently incorporated into any hydrodynamic modeling tools.

To help balance performance and environmental drivers there is a need to develop verified and validated simulation approaches capable of predicting power output along with any environmental changes from a CEC array. For these approaches to be beneficial for developers, this type of modeling must provide turnaround times for month-long simulations in a matter of hours, while facilitating investigation of regional-scale hydrodynamic and environmental effects, (i.e., on domains spanning tens to hundreds of kilometers). In response to this need, Sandia National Laboratories (SNL) has developed and implemented a new capability into an existing flow, sediment-dynamics, and water-quality code (EFDC [21,22], now SNL-EFDC [23]) to quantify and visualize the interaction and influence of CEC devices in arbitrary flow systems. In this study, the power production of the model is first verified through comparison to an analytical solution in a simplified, two dimensional tidal channel as a function of flow rate [4]. Three laboratory flume experiments are used to calibrate turbulence parameters for use in CEC-specific applications. It is anticipated that a single set of parameters may be usable for CEC simulations, as has been seen in simulations for flow through vegetative canopies [24] and wind turbines [25]. SNL-EFDC is an open-source tool that can determine the power generated and effects of CEC arrays on system circulation, sediment dynamics, and water quality, thereby providing a platform to understand their environmental impacts at regional scales.

2. Methods

2.1. Modeling framework

SNL-EFDC is a modified version of US Environmental Protection Agency's Environmental Fluid Dynamics Code [21,22], coupled to both the US Army Corps of Engineers' water-quality code, CE-QUAL-ICM (Quality Integrated Compartment Model) [26,27], and the sediment-dynamics code, SEDZLJ [28,29]. EFDC was developed to study river-, estuary-, coastal-, and ocean-scale systems. It also includes routines for vegetative resistance and wetting and drying of wetlands regions. EFDC has recently been implemented in a parallel computing environment [30,31].

The hydrodynamic portion of EFDC solves the hydrostatic, free-surface Reynolds-averaged Navier Stokes (RANS) equations with Mellor-Yamada turbulence closure [32] as modified by Galperin, Kantha, Hassid and Rosati [33]. This is similar to the model of Blumberg and Mellor [34] except for the solution of the free surface, which is solved with a preconditioned conjugate gradient solver. EFDC uses a curvilinear-orthogonal grid with a sigma vertical coordinate system [21,22]. The number of sigma layers is fixed for each model and assigned a constant (often equal) fraction of the flow depth throughout the model domain, where the local thickness of each layer changes with the topology of the model domain and water depth. EFDC's time integration uses a second-order-accurate finite-difference scheme with an internal/external mode-splitting procedure to separate the internal shear (or baroclinic mode calculated across each sigma layer) from the external free-surface gravity wave (or barotropic mode calculated on the depth average). EFDC has been extensively applied, validated, and documented at numerous sites worldwide, including estuaries, wetlands, lakes, rivers, and coastal environments [35–38]. The model has also been validated against analytical solutions, laboratory experiments, and real flow systems [39,40].

This effort introduces and presents a new SNL-EFDC module that considers momentum (energy) removal from the flow system by CEC devices and the commensurate changes to the momentum balance and turbulent kinetic energy and its length scale (or dissipation rate) [41,42]. The CEC module provides a design approach capable of rapidly predicting hydrodynamic changes resulting from power production from field-scale CEC array configurations. This modeling approach is not intended to provide high-fidelity simulations of rotor hydrodynamics or detailed turbine wake structures. Once a desired array layout has been identified using SNL-EFDC, more detailed CFD simulations can be performed [43–45]. It is acknowledged that waves may impact CEC wakes [46,47], but these effects are not considered in this work because none of the flume experiments implemented waves.

2.2. Current-energy converter simulation module

The CEC module simulates removal of energy by turbines based on device-specific performance metrics through a reduction in momentum in model cells where devices are situated. Corresponding changes to turbulent kinetic energy and turbulence length scale are implemented similarly to changes through a vegetative canopy [48], which has been successfully applied to the wind-energy community [25,49]. Density-normalized source/sink terms, S_Q (m^4/s^2), S_k (m^5/s^3), and S_ℓ (m^6/s^3) represent the rate of momentum reduction, net change to turbulence intensity, and the increase in turbulence length scale, respectively, are [50]:

$$S_Q = \frac{1}{2} C_T' A U^2, \tag{1}$$

$$S_k = \frac{1}{2} C_T' A \left(\beta_p U^3 - \beta_d U k \right), \tag{2}$$

$$S_\ell = C_{\ell 4} \ell S_k, \tag{3}$$

where C_T' (−) is the modified (see below) thrust coefficient (or a constant drag coefficient, C_D, for support structures), U (m/s) is the undisturbed, local, free-stream flow speed, and A (m^2) is the flow-facing area of the turbine blades/support structure. k (m^2/s^2) is the mean-flow kinetic energy, and β_p (−) is the fraction of k converted to wake-generated kinetic energy by drag, which accounts for the production of wake turbulence and represents the ratio of mean kinetic energy transferred directly into turbulence (not the shear-generated turbulence). β_d (−) accounts for k dissipation through conversion to kinetic energy of the turbine blades, or the short-circuiting of the turbulence cascade where energy transfers from large-scale turbulence to smaller scales. The turbulence length scale is ℓ (m) and $C_{\ell 4}$ (−) is a closure constant [51]. For vegetative canopies, Katul, Mahrt, Poggi and Sanz [24] suggest $\beta_p = 1$, $\beta_d = 1–5$, and $C_{\ell 4} = 0.9$, while for wind turbines Réthoré, Sørensen

Please cite this article in press as: S.C. James, et al., Simulating current-energy converters: SNL-EFDC model development, verification, and parameter estimation, Renewable Energy (2017), http://dx.doi.org/10.1016/j.renene.2017.07.020

and Zahle [25] suggest $\beta_p = 0.05$, $\beta_d = 1.5$, and $C_{\ell 4} = 1.6$. These values are not directly transferrable to CEC devices because of density and viscosity differences between the media, existence of the free surface, and effects of the device on downstream turbulence (e.g., the difference between horizontal- and vertical-axis turbines). Instead, these parameters can be calibrated to available data sets. The effects of affiliated support structures are similarly considered.

Two additional parameters, α_{md} and K_v, must be specified when using surface-water flow models like EFDC, where α_{md} describes horizontal momentum diffusion [52] and K_v specifies vertical momentum diffusion in the system. Each serves to damp velocity gradients in the horizontal and vertical (e.g., the wake structure behind a CEC device). Specifically, α_{md} is a multiplier on the horizontal stress tensor [22, Eqns. (55)–(57)] in the solution of the horizontal momentum conservation equations. It represents subgrid-scale turbulent mixing and also serves to smooth cell-to-cell spatial oscillations in the numerical solution in proportion to the local horizontal strain rate [52]. As a rule of thumb, the Smagorinsky constant should scale with the inverse square root of cell size, where a reasonable approximation for EFDC modeling is about one-thousandth of the average cell area in square meters when cells exceed 10×10 m^2. This generality does not apply to models with grid cells smaller than a square meter, as used in these flume models, and is therefore a calibrated parameter. K_v is the vertical turbulent eddy viscosity, which appears in the vertical diffusive term in the horizontal momentum and k-$k\ell$ turbulence equations [22, Eqns. (2), (3), (13) and (14)]. These two parameter are commonly calibrated for every surface-water model [37].

Equations (1) and (2) require the undisturbed flow speed; however, the presence of the device alters the local flow field. The local velocity at the device can be used instead, but requires modification of the device-specific, velocity-dependent, thrust coefficient [53]:

$$C'_T = 4\frac{1-\sqrt{1-C_T}}{1+\sqrt{1-C_T}}. \tag{4}$$

Momentum theory applied to a streamtube fully encompassing a horizontal-axis turbine does not allow for the wake to re-energize. The upper bound for C_T is equal to 1 when derived through momentum theory whereupon a zero velocity occurs in the wake and as C_T increases further the wake velocity reverses. The power generated by a turbine is proportional to the thrust and can be estimated using the modified thrust coefficient as:

$$P = \frac{1}{2}\rho A C'_T U_d^3, \tag{5}$$

where ρ (kg/m^3) is the fluid density and U_d is the local velocity at the device.

3. Verification of power production

3.1. Analytical solution for a tidal channel

A two-dimensional tidal channel with a CEC fence of increasing density (number of turbines per cell) was simulated with SNL-EFDC to estimate the power generated and the hydrodynamic response. The fence represents a uniform, porous obstruction to flow at a cross section of the channel and does not explicitly consider individual turbines or allow for flow acceleration around the fence and in two dimensions (single model layer) there can be no flow over or under the fence. This representation provides a means to verify the energy removed by any number of turbines in the model without regard to the other parameters or wake re-energization. Garrett and Cummins [4] present an analytical solution to this problem describing the instantaneous power potential of tidal currents in channels:

$$P = \rho Q(g\zeta - \alpha Q|Q|), \tag{6}$$

where Q (m^3/s) is instantaneous flow rate, g (m/s^2) is gravity, ζ (m) is the surface elevation difference between the two ends of the channel, and α (1/m^4) is a measure of the channel friction and flow separation at the ends. For a specified tidal prism, a maximum undisturbed flow rate exists for the channel and the total power produced initially increases as CECs are added. However, the added turbines also increase a resistance to the flow, ultimately reducing the overall flow rate. These two competing trends dictate that maximum power production cannot occur when the flow rate is at its maximum. The analytical solution predicts maximum power generation when the CEC resistance reduces the flow rate to 57.7% of the maximum. The maximum average power that can be generated from a tidal-channel system is then [4]:

$$\overline{P}_{max} = \gamma \rho g a Q_{max}, \tag{7}$$

where γ (−) is a coefficient between 0.21 and 0.24 that incorporates the time average of a harmonic tidal range, bed friction, and separation at the channel ends, a (m) is the tidal amplitude between the ends of the channel, and Q_{max} (m^3/s) is the maximum flow rate through the channel when undisturbed. As recommended by Garrett and Cummins [4], γ was set equal to 0.22, allowing a 10% margin in power accuracy.

3.2. Simulation description

Using the geometry and domain setup specified by Yang, Wang and Copping [54], a tidal channel was developed for SNL-EFDC, shown in Fig. 1 and colored by depth. The dimensions of the system are listed in Table 1 and the bottom roughness was set to 2 cm. A sinusoidal, M2 tidal forcing with a 1-m amplitude was applied on the open-ocean boundary to the west and drives the surface elevation difference between both ends of the channel. For simplicity, and to compare most directly to the results of Garrett and Cummins [4], the simulation was two-dimensional (a single layer in the vertical, which does not consider flow above or below the devices) with a fence of turbines spanning the entire width of the channel. Fig. 2 indicates the location of the CEC fence where the number of turbines was varied uniformly in each of the 20 cells across the channel. Turbine resistance is treated as a porous obstruction where the momentum sink considers the turbine size (10-m diameter) and thrust coefficient ($C_T = 0.5$). Assuming frictionless side walls, turbulence and flow parameters β_p, β_d, $C_{\ell 4}$, α_{md}, and K_v have no effect on the power, flow rate, or wake recovery in a two-dimensional model; only the momentum sink, S_Q, drives the system's response.

3.3. Discussion

The model initially ran with a turbine density of zero to replicate the unobstructed channel. This resulted in a maximum flow speed of 2.64 m/s and a predicted maximum average flow power of 2.10 GW. Turbine density was then increased as the flow rate and power generation were recorded. Fig. 3 shows that the SNL-EFDC model closely replicates the analytical solution of normalized power production [4,54]. The predicted maximum power from SNL-EFDC was generated when the flow rate was 57.3% of its maximum. This corresponds to a maximum average flow power of

Please cite this article in press as: S.C. James, et al., Simulating current-energy converters: SNL-EFDC model development, verification, and parameter estimation, Renewable Energy (2017), http://dx.doi.org/10.1016/j.renene.2017.07.020

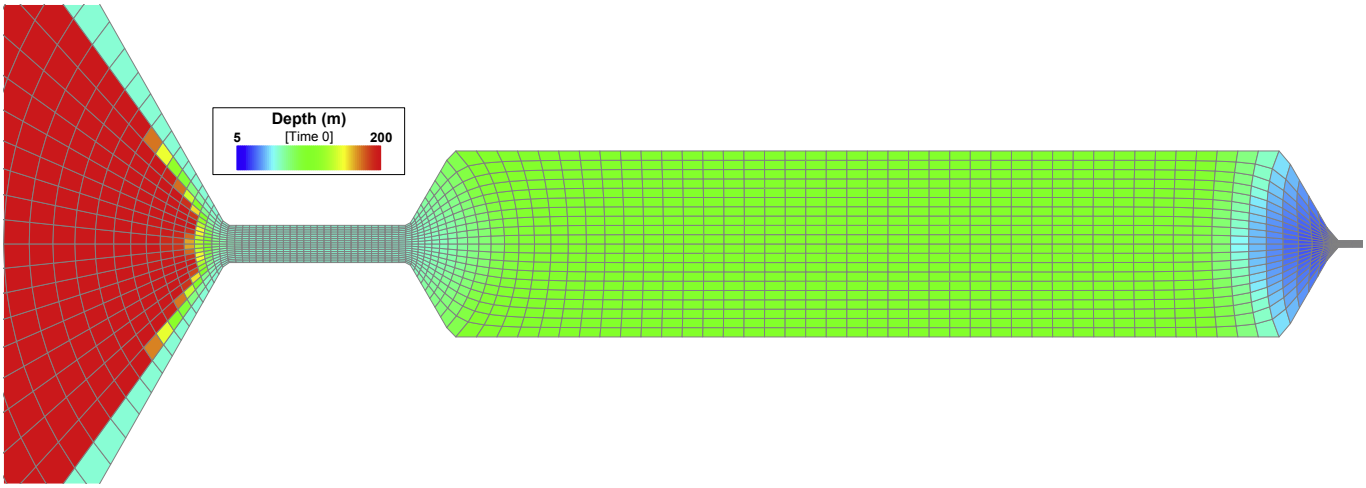

Fig. 1. Grid with depth (color) of the tidal channel. (For interpretation of the references to color in this figure legend, the reader is referred to the web version of this article.)

Table 1
Tidal-channel dimensions.

Location	Length (m)	Width (m)	Depth (m)
Open ocean	165,000	260,000	200
Tidal channel	30,000	6000	60
Semi-enclosed bay	150,000	30,000	100

2.00 GW and an instantaneous maximum near 4.72 GW. The small difference between the analytical and model results can be accounted for by model approximations; the M2 tidal condition is enforced at one end of the domain instead of being a strict value across the channel, γ is held constant instead of being allowed to vary, and the single σ layer prevents any potential flow separation. Similar results were reported by Yang, Wang and Copping [54] with CEC modifications to their FVCOM model [55].

4. Turbulence parameter calibration

The tidal fence represents idealized energy removal in a tidal straight and the two-dimensional approximation cannot account for the complex flow around and behind each device. Having verified that energy removed by CEC devices is accurately simulated, the k-$k\ell$ source equations, (2) and (3), become impactful in the following three-dimensional models and impact re-energization of the wake. Without their consideration, the wake would be overly persistent. Three experiments were used to calibrate those parameters for CEC-specific modeling.

4.1. Experiment and simulation descriptions

The five adjustable model parameters were calibrated against three experimental data sets to investigate trends across the available experimental systems and data. The first data set is for an actuator-disc experiment conducted in the Chilworth flume at the University of Southampton in the UK [56]. Actuator discs have been shown to accurately represent the thrust load and wake deficit of horizontal-axis turbines [57], but are unable to induce the same vortical structure seen in both horizontal-axis and cross-flow turbines. The second and third sets of experimental data are from

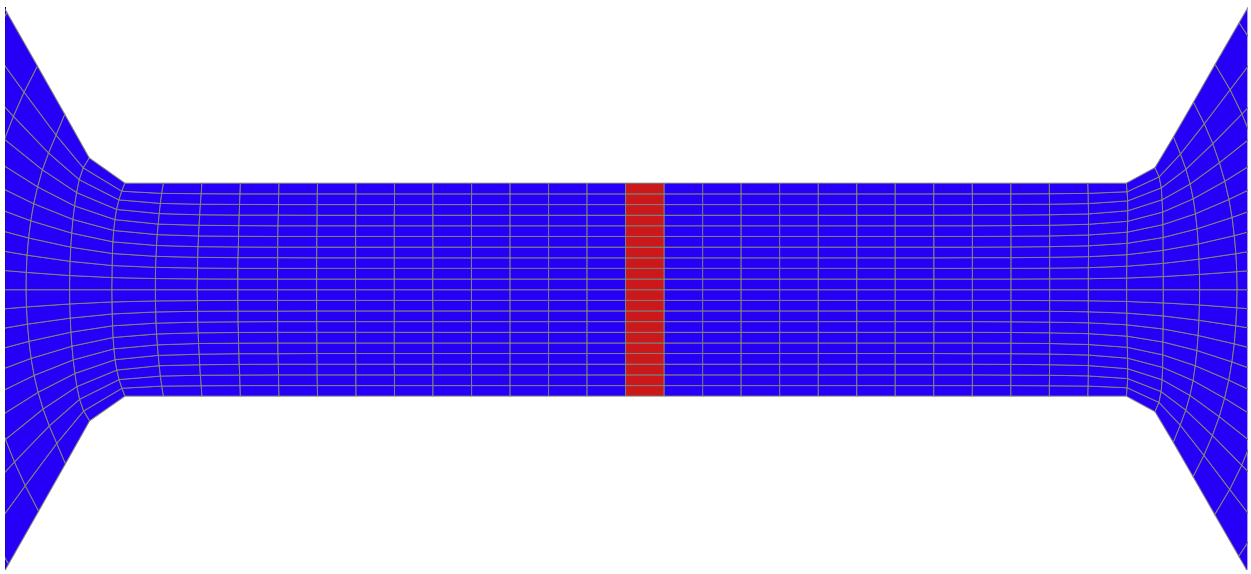

Fig. 2. Location of the CEC fence across 20 cells in the throat of the tidal channel.

Please cite this article in press as: S.C. James, et al., Simulating current-energy converters: SNL-EFDC model development, verification, and parameter estimation, Renewable Energy (2017), http://dx.doi.org/10.1016/j.renene.2017.07.020

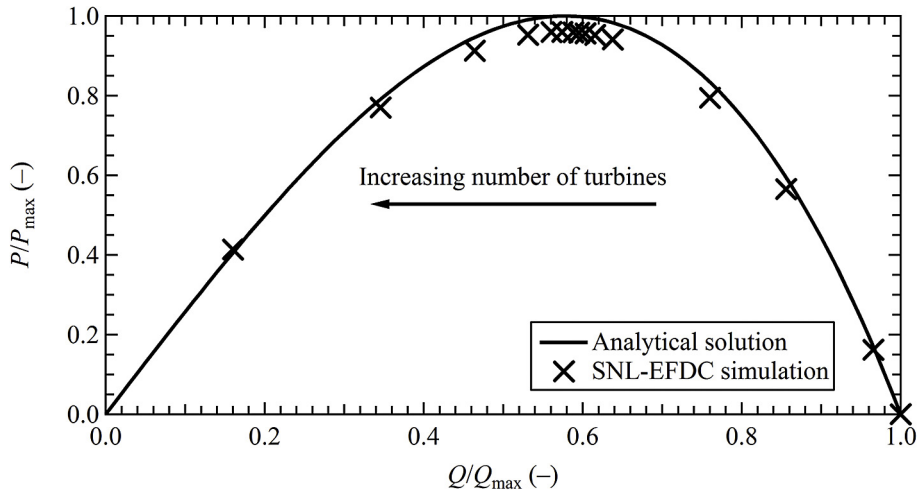

Fig. 3. Comparison of the Garrett and Cummins [4] analytical solution (curve) for power withdrawal (P/P_{max}) as a function of normalized volumetric flow rate to the SNL-EFDC simulations (symbols).

scaled-turbine tests conducted in the IFREMER circulating water channel at Boulogne-sur-Mer in France [58] and at Saint Anthony Fall Laboratory (SAFL) at the University of Minnesota [59]. Table 2 describes each of the channels and discs/rotors used in the flume experiments.

For each of the models, uniform flows are specified at the flume inlets and constant water elevations are specified at the outlets. The particular model characteristics are listed in Table 3. Note that the modeled flume did not need to be as long as the actual flumes because data were only collected to 25 device diameters downstream and there was no need to model any further distances. Flume roughnesses were specified as 2 mm as appropriate for cement-bottom flumes. Using the average x velocity along a lateral transect five device diameters downstream from the turbine at hub height as the performance metric, grid-convergence indices were 3.8%, 3.2%, and 3.4% for the IFREMER, SAFL, and Chilworth models, respectively, which, according to Roache [60], Table 1, are considered acceptable. For these studies, the grid refinement ratio was two (in the horizontal only) and SNL-EFDC is second-order accurate in space.

4.2. Experimental data

For each experiment, the wake structure was characterized by up to four observation groups: (1) hub-height, centerline velocities at increasing distances downstream (longitudinal velocity profiles), (2) cross-wake velocities at one or more distances downstream (lateral velocity profiles), (3) depth-dependent velocities at one or more longitudinal distances downstream (vertical velocity profiles), and (4) turbulence intensities with distance downstream or in vertical profiles. Table 4 lists the available data for each experiment.

Data are reported as measured velocity, or more often as a velocity deficit, the dimensionless ratio of the wake velocity at any location downstream of the CEC, U_w, to the free-stream flow speed, U_∞:

$$U_{def} = 1 - \frac{U_w}{U_\infty}. \tag{8}$$

The velocity deficit downstream of the rotor plane and along the CEC centerline decreases, on average, from about 60% at three device diameters downstream of the rotor plane to about 20–25% at 10 device diameters, 10D. Other studies indicate a recovery to 10% deficit within 15–20 device diameters downstream [56,62,66]. Because the converted power is proportional to the cube of the incoming velocity, optimal device spacing and arrangement for power performance is highly dependent upon the distance required for the wake to recover. The velocity deficit in the near-wake of a turbine (less than approximately three device diameters) is highly unstructured due to the turbulent flow shed from the hub/nacelle and turbine-blade roots and the velocity measurements fluctuate significantly.

4.3. Parameter estimation strategy

PEST (Parameter ESTimation) [67,68] was used to calibrate turbulence and flow parameters. PEST conducts gradient-based, nonlinear parameter estimation, based on the Gauss-Marquardt-Levenberg algorithm, and adjusts model parameters to minimize a weighted, least-squares objective function. PEST has also been applied for uncertainty assessments and sensitivity analyses [69]. For this study, calibration parameters are the three turbulence parameters (β_p, β_d, and $C_{\ell 4}$) and the two flow (momentum diffusion) parameters (α_{md} and K_v). A single set of turbulence parameters were calibrated for all three flume models because universal values are sought for flume experiments. Independent flow

Table 2
Experimental descriptions.

Experiment	Channel			Rotor			Support Structure		
	Length (m)	Width (m)	Water depth (m)	Type	Diameter (m)	$C_T(-)$	Height (m)	Width (m)	$C_D(-)$
Chilworth	21	1.35	0.3	Actuator disc	0.1	0.86	0.264	0.01	1.2
IFREMER	18	4	2	3-bladed turbine	0.8	0.77	0.94	0.1	1.2
SAFL	85	2.75	1.155	3-bladed turbine	0.5	0.58	0.425	0.1	1.2

Please cite this article in press as: S.C. James, et al., Simulating current-energy converters: SNL-EFDC model development, verification, and parameter estimation, Renewable Energy (2017), http://dx.doi.org/10.1016/j.renene.2017.07.020

Table 3
Model descriptions.

Model	Nominal grid cell size (cm^2)	Number of cells	Number of layers	Total length and width (m^2)	Depth (m)	Average flow speed (m/s)	Roughness (mm)
Chilworth	3.3 × 3.3	8610	27	6.3 × 1.35	0.3	0.28	2
IFREMER	16 × 16	2750	25	17.6 × 4	2.0	0.8	2
SAFL	10 × 10	4050	59	15 × 2.75	1.155	0.4	2

Table 4
Available data from each flume experiment.

Experiment	Longitudinal profile	Lateral profiles	Vertical profiles	Turbulence intensity
Chilworth	[56, Fig. 8]	[61, Fig. 16, 62, Fig. 5c]	[61, Fig. 15, 62, Fig. 5a]	[56, Fig. 12, 62, Figs. 5b,d]
IFREMER	[63, Fig. 9]	[63, Fig. 7]	[63, Fig. 8]	[64, Fig. 8]
SAFL	[65, Fig. 5]	Personal communication	[65, Fig. 2]	[65, Figs. 4 and 6]

parameters were calibrated simultaneously for each model because the varied flow rates, widths, and depths require unique estimates of these. The objective function is defined as the weighted sum of squared differences between measured velocity deficits and turbulence intensities (U^*_{def} and TI^*) and their simulated equivalents (U_{def} and TI):

$$\Phi = \sum_i w_i \left(U^*_{\mathrm{def}} - U_{\mathrm{def}}\right)^2_i + \sum_j w_j (TI^* - TI)^2_j, \tag{9}$$

where w is the weight. Weights were user-specified and consider factors such as the importance of matching near- and far-wake velocity deficits. Because the model does not consider physical displacement of fluid by the turbine and support structure, all data points within the near wake (less than or equal to three device diameters) were weighted to $w = 0$. Weights were increased near the tails of the longitudinal profiles to ensure that PEST honors these data and simulates a realistic wake recovery because the far wake is much more crucial for siting. Turbulence intensities were weighted to $w = 0.1$ because these data were less certain and because the primary goal of this effort is to accurately simulate wake characteristics and not turbulence profiles.

Preliminary investigations revealed that the adjustable parameters could not uniquely be determined from only the longitudinal (centerline) velocity profile as it is not primarily sensitive to the turbulence parameters (β_{p}, β_{d}, and $C_{\ell 4}$). This led to many combinations of α_{md}, and K_{v} that calibrated the model equally well. Inclusion of lateral and vertical velocity profiles and turbulence intensities in the objective function was necessary to uniquely estimate the parameters. This is unsurprising given that the lateral spreading of the wake depends upon diffusion through both global and device-generated turbulence. Unlike a natural system where α_{md} and K_{v} would be calibrated against data from the undisturbed system, α_{md} cannot be calibrated against uniform channel flows where no horizontal velocity gradients exist in the main body of the flow. Because undisturbed vertical velocity and turbulence intensity profiles are available for the Chilworth and SAFL flumes, these were first used to establish an initial, preferred value for $K_{\mathrm{v}} = 3.2 \times 10^{-4}$ m^2/s [53] and the initial turbulence parameter values came from Réthoré, Sørensen and Zahle [25].

4.4. Parameter estimation results

The best-fit turbulence and flow parameters for each model are listed in Table 5 and Figs. 4–6 compare the PEST fits to each of the three experimental data sets. While PEST also reports parameter sensitivities as the change in objective function per unit change in parameter, it is difficult to interpret such values given that a unified set of turbulence parameters was sought and because calibration was across models of all three experiments at once. For example, because each model contributes individually to the overall objective function, but flow parameters only impact one model at a time, this obscures their sensitivities, especially with respect to the turbulence parameters, which impact all three models at once.

4.4.1. Fit to the Chilworth actuator disc experiment

Fig. 4 compares the PEST fits to the data collected from the Chilworth actuator-disc flume experiment. Fig. 4(a) compares the measured longitudinal U_{def} profile (symbols) and best fit (curve) from 3 to 20D downstream. The simulated longitudinal velocity deficits match the measured Chilworth data well because, as with the experiment, the CEC module represents the turbine as an actuator disc, ignoring blade shape and nacelle obstruction. Fig. 4(b) presents lateral U_{def} profiles at transects from 3 to 7D downstream. At about 1.8D in the lateral direction, the best-fit, hub-height U_{def} curves become negative, indicating the local velocity is faster than the hub-height free-stream velocity at the inlet. However, this is consistent with conservation of mass and SNL-EFDC demonstrating a persistent deficit over the experimental values near the free-surface, Fig. 4(c). As the measured data do not show a similar increase in velocity near the walls, this could be due to a slight error in the reported downstream water level that is not

Table 5
Calibrated model parameters compared to previous values for vegetative canopies and wind turbine applications.

Parameter	Chilworth	IFREMER	SAFL	Vegetative [24]	Wind turbine [25]
β_{p} (−)[a]		←0.96→		1.0	0.05
β_{d} (−)[a]		←1.38→		1.0–5.0	1.5
$C_{\varepsilon 4}$ (−)[a]		←3.87→		0.9	1.6
α_{md} (m^2/s)[b]	1.7	1.1	1.5		
K_{v} (m^2/s)[b]	1.6×10^{-4}	4.7×10^{-4}	5.0×10^{-4}		

[a] Turbulence parameter (global).
[b] Flow parameter (system specific).

Please cite this article in press as: S.C. James, et al., Simulating current-energy converters: SNL-EFDC model development, verification, and parameter estimation, Renewable Energy (2017), http://dx.doi.org/10.1016/j.renene.2017.07.020

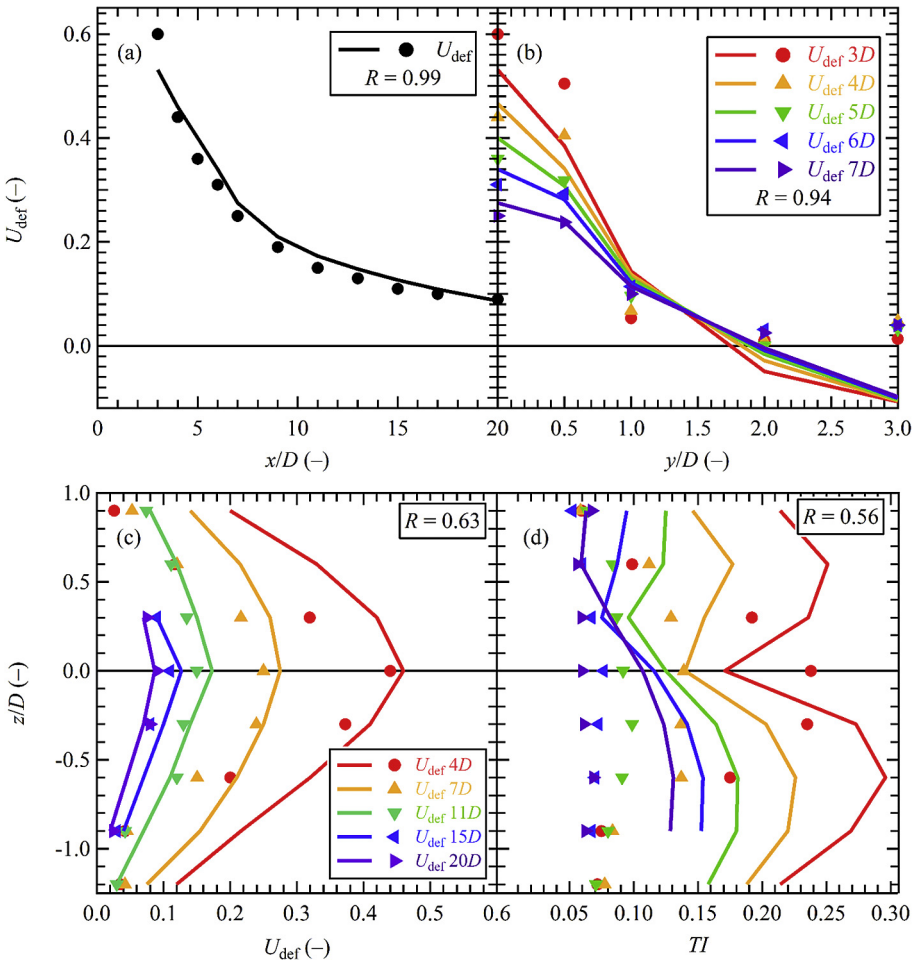

Fig. 4. PEST fits (curves) to the Chilworth data (symbols) for (a) hub-height longitudinal U_{def} profile (3–20*D*), (b) hub-height lateral U_{def} profiles (3–7*D*), (c) vertical U_{def} profiles (4–20*D*), and (d) and vertical *TI* profiles (4–20*D*). Flow is from left to right in (a), (c), (d) and from bottom to top in (b).

represented in the model because the outlet pressure condition is set to the reported depth listed in Table 2. Fig. 4(c) compares vertical U_{def} profiles at transects from 4 to 20*D* downstream. Fig. 4(d) presents vertical *TI* profiles at transects from 4 to 20*D*. Noteworthy is that simulated *TI*s are low along the disc centerline, which is consistent for introduction of *TI* at locations of high velocity gradients around the edges of a disc. While the Chilworth experimental data show only one location of increased *TI* directly behind the disc, this is different from the bi-modal pattern reported by Stallard, Collings, Feng and Whelan [70] and seen in the SNL-EFDC results. Note that the correlation coefficients, *R*, listed on the figures are fairly strong for the velocity deficits but weaker for *TI*. This is due in part because *TI* data were not weighted as heavily during calibration and because the RANS formulation and the numerical grid inherently limit how well these derived quantities can be matched.

4.4.2. Fit to the IFREMER scaled-turbine experiment

Fig. 5 shows the PEST fits to the data collected from the IFREMER flume experiment. Fig. 5(a) shows the measured longitudinal U_{def} profile (blue squares) and best fit (blue curve) from 3 to 14*D* downstream on the left axis and *TI* (red circles) and best fit (red curve) from 5 to 10*D* downstream on the right axis. Fig. 5(b) shows the lateral U_{def} profiles from ±0.2*D* in the vertical in increments of 0.1*D* at a distance of 5*D* downstream from the turbine. Fig. 5(c) shows the vertical U_{def} profile at a distance of 5*D* downstream from the turbine. There are inflection points in the vertical U_{def} profile toward both the bottom and top of the flume. While the inflection point near the bottom of the flume is due to boundary layer development, the measured U_{def} deviation near the water surface is likely due to inherent limitations of ADCP measurements near the free surface. As a result, the top two data points in the vertical profile were not weighted during calibration. Note that the predicted centerline U_{def} for both the lateral and vertical profiles, Fig. 5(b) and (c), demonstrate slight underestimates of the velocity deficit as the wake is re-energized by the surrounding flow, but the centerline velocities are captured well as inferred from Fig. 5(a) where $R = 0.98$. A contributing factor as to why the peak deficit is not achieved is because the turbine hub is not explicitly represented in SNL-EFDC, which represents turbines as porous blockages instead of requiring zero normal velocities at turbine structures. Nevertheless, the correlation coefficients indicate that the model simulates the wake characteristics of this turbine well, especially for the longitudinal velocity profile, which is important to know so that devices can be optimally spaced in an array.

4.4.3. Fit to the SAFL scaled-turbine experiment

Fig. 6 compares the PEST fits to the data collected from the SAFL flume experiment. Fig. 6(a) shows the measured longitudinal U_{def} profile downstream from the turbine centerline and edge of the turbine blades (blue and red curves, respectively) from 1 to 20*D* downstream. The model slightly under-predicts U_{def} in the near-

Please cite this article in press as: S.C. James, et al., Simulating current-energy converters: SNL-EFDC model development, verification, and parameter estimation, Renewable Energy (2017), http://dx.doi.org/10.1016/j.renene.2017.07.020

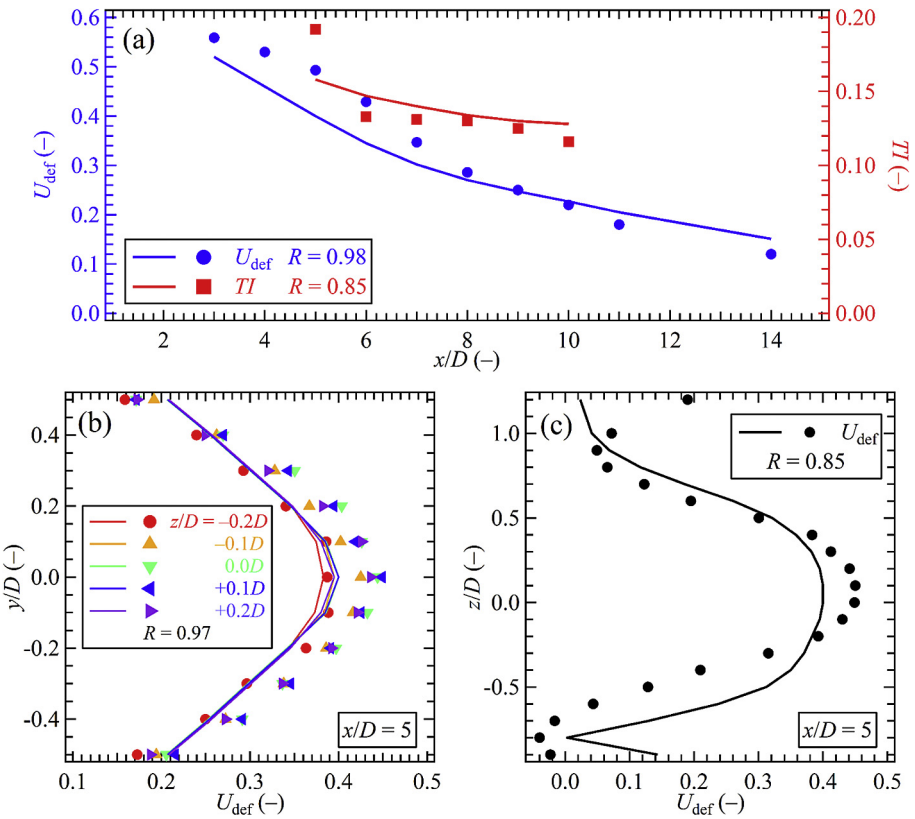

Fig. 5. PEST fits (curves) to the IFREMER data (symbols) for (a) longitudinal U_{def} profile (3–14*D*) and *TI* profile (5–10*D*), (b) lateral U_{def} profiles at 5*D*, and (c) vertical U_{def} profiles at 5*D*. Flow is from left to right in all panels.

wake region of the rotor (<3*D* downstream), but this is partially due to U_{def} and *TI* being weighted to $w = 0$ in this region where SNL-EFDC is not anticipated to replicate the complex flows immediately downstream of the turbine/disc. Nevertheless, the maximum velocity deficit and trend within the near wake are still captured. Fig. 6(b) compare the measured vertical U_{def} (bottom *x* axis) and *TI* (top *x* axis) profiles at distances of −1, 1, 3, 5, 9, and 15*D* downstream from the turbine, respectively. Note that $x/D = -1$ is one device diameter upstream of the turbine. Similar to the Chilworth and IFREMER fits, correlation coefficients are higher for velocity deficits than for *TI*.

4.5. Discussion

Given that there are necessarily uncertainties in the measured data, the overall calibrations are acceptable and indicate that SNL-EFDC can be used to replicate flume experiments if baseline measures of the horizontal and vertical momentum diffusivities are known or calibrated. Consistent with the experimental data, the new CEC module predicts an approximate 60% decrease in velocity in the lee of the device with a wake recovery to within 10% of the freestream between 15 and 20*D*. Similarly, *TI* abruptly increases in the near-wake and dissipates to background levels within 10*D*. Despite increased system and measurement uncertainties in real-world systems, SNL-EFDC has recently been used to optimize array layouts [71]. In addition, the amount of simulation information produced for the low computational expense is notable, especially given that techniques are available to parallelize EFDC [30,31] or to run it on cloud computing systems [72].

Calibrated parameter values control the fit between experimental data and simulations. Some of the model-to-measurement misfit is incurred when one observation group is better fit at the expense of another. Because the implementation of the *k-kℓ* turbulence model within SNL-EFDC was formulated for geographic-scale obstructions, and not sub-grid-scale devices, the high, local shears and turbulence introduced by CEC devices are difficult to simulate. Because of this uncertainty, all *TI* data were weighted about an order of magnitude less than their U_{def} counterparts. Moreover, parameter covariance can complicate estimated parameter values. This means that the ratio of covarying parameters could be more accurately estimated than their individual values. Also, because PEST was used to fit all parameters simultaneously, the gradient-based approach may have found a local minimum, even though PEST [67,68] and the authors attempted to step out of such valleys (e.g., through PEST's regularization techniques and by the authors using appropriate initial parameter values). While there is correlation in estimated parameters across experiments, α_{md} and K_v should be calibrated first in a system without CEC devices. Data collection for such a calibration effort is currently underway at a field site [73,74].

Overall, the vegetative-canopy model for momentum loss and turbulence generation implemented in SNL-EFDC shows some deficiencies in predicting the flows directly behind CEC devices in experimental flumes. Specifically, gradients in velocity deficits were often under-predicted in the lateral and vertical profiles. This indicates model structural error [75], which is the inability of a model to capture the true complexity of a physical system because the model is necessarily a simplification of reality and inherent deficiencies in representing complex geometries of the CEC obstructions (they act as porous barriers to flow). Moreover, SNL-EFDC is limited to a single, global value for the Smagorinsky constant, α_{md}. It is more likely that α_{md} (and K_v as well) vary spatially and

Please cite this article in press as: S.C. James, et al., Simulating current-energy converters: SNL-EFDC model development, verification, and parameter estimation, Renewable Energy (2017), http://dx.doi.org/10.1016/j.renene.2017.07.020

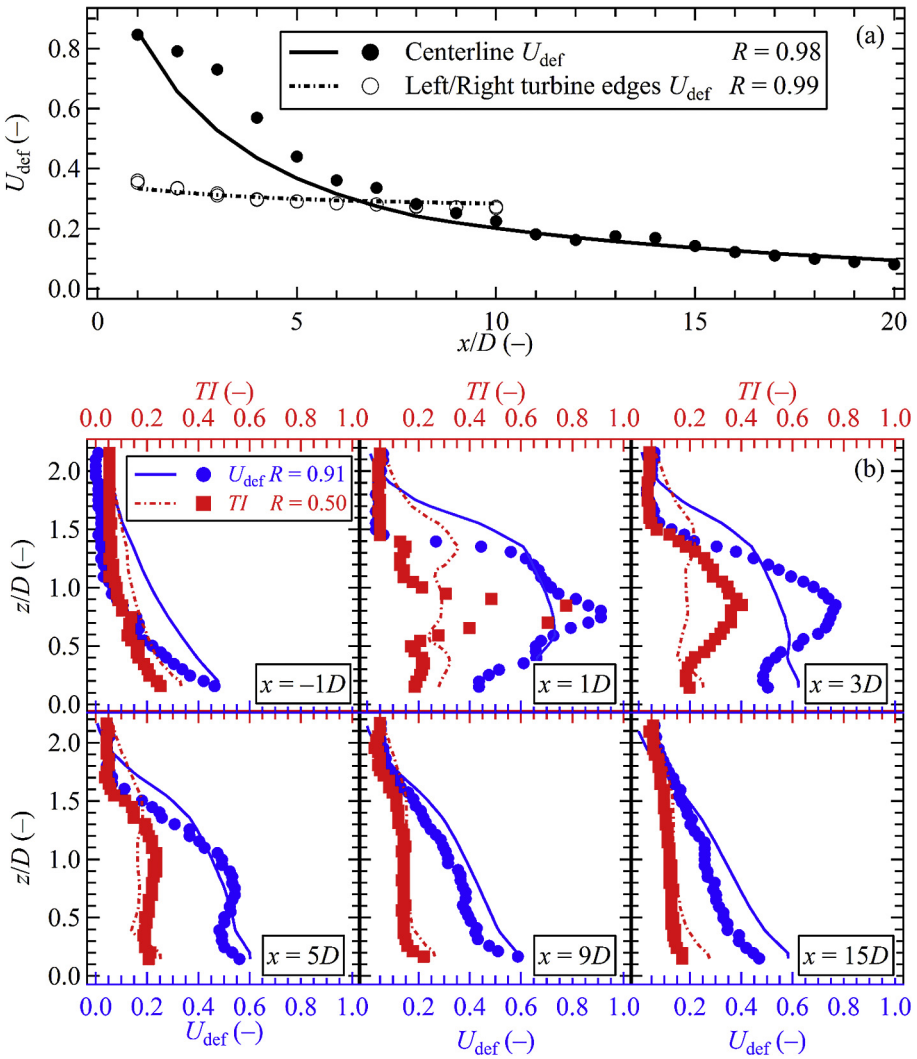

Fig. 6. PEST fits (curves) to the SAFL data (symbols) for (a) longitudinal U_{def} profiles (1–20D) and (b) vertical U_{def} profiles at −1, 1, 3, 5, 9, and 15D (bottom x axis) and vertical TI profiles at −1, 1, 3, 5, 9, and 15D (top x axis). Flow is from left to right in all panels.

have different values in the free stream than in the wake. To the degree that parameters can compensate for model structural error, parameters may deviate from their measured physical value. Blackmore, Batten and Bahaj [76] have indicated the importance of background TI in wake recovery. Without being able to match background TI in the models because such data were not available from these experiments, it is expected that estimated parameters may deviate from their true values in an attempt to compensate for model structural error.

5. Conclusions

A CEC module was incorporated into SNL-EFDC using a momentum sink approach with commensurate adjustments to the k-$k\ell$ turbulence transport equations. This facilitates simulation of power generation from CEC turbines at a regional flow scale while including local-scale changes due to momentum removal. The CEC module permits the use of different devices (i.e., varying size and thrust coefficient) in an arbitrary flow system. An analytic solution for power generation through a tidally forced channel was replicated with SNL-EFDC, which verified that maximum power production occurs when there is a reduction to 57% in the maximum channel flow. A single set of empirical turbulence parameters required to replicate wake characteristics of in-stream devices were calibrated to match the wakes from three different experiments. Through inclusion of the CEC module into SNL-EFDC, hydrodynamic and environmental studies and optimizations can be performed simultaneously and tractably within a single modeling framework. This allows users to assess how increased power generation affects hydrodynamics, sediment dynamics, and even temperature and water quality. SNL-EFDC is an open-source code available to researchers, regulators, and the industry.

Future work will build upon the calibration framework developed here and compare the device parameters estimated from flume experiments to parameters estimated for a full-scale vertical axis turbine. This will reveal the degree to which parameters are device-specific and relevant across domains and scales. Also, because SNL-EFDC has both sediment-dynamics and water-quality modules, this modeling platform can easily be extended to addressing CEC impacts on these processes.

Acknowledgements

Sandia National Laboratories is a multi-mission laboratory

managed and operated by National Technology and Engineering Solutions of Sandia, LLC., a wholly owned subsidiary of Honeywell International, Inc., for the U.S. Department of Energy's National Nuclear Security Administration under contract DE-NA0003525.

This research was made possible by support from the Department of Energy's Energy Efficiency and Renewable Energy Office's Wind and Water Power Program.

EFDC Explorer [77] was used to visualize some of the model results.

The authors gratefully acknowledge four Baylor University undergraduate researchers who helped with the calibration efforts in this manuscript: Andrew Duke, Nicklas Keller, Jackson Liller, and Samantha Simpson.

References

[1] I.G. Bryden, S.J. Couch, A. Owen, G. Melville, Tidal current resource assessment, J. Power Energy 221 (2007) 125–135.
[2] R. Inger, M.J. Attrill, S. Bearhop, A.C. Broderick, W.J. Grecian, D.J. Hodgson, C. Mills, E. Sheehan, S.C. Votier, M.J. Witt, B.J. Godley, Marine renewable energy: Potential benefits to biodiversity? An urgent call for research, J. Appl. Ecol. 46 (2009) 1145–1153.
[3] B. Polagye, M. Kawase, P. Malte, In-stream tidal energy potential of Puget Sound, Washington, Proc. Inst. Mech. Eng. Part A J. Power Energy 223 (2009) 571–587.
[4] C. Garrett, P. Cummins, The power potential of tidal currents in channels, Proc. R. Soc. A Math. Phys. Eng. Sci. 461 (2005) 2563–2572.
[5] D. Hasegawa, J. Sheng, D.A. Greenberg, K.R. Thompson, Far-field effects of tidal energy extraction in the Minas Passage on tidal circulation in the Bay of Fundy and Gulf of Maine using a nested-grid coastal circulation model, Ocean Dyn. 61 (2011) 1845–1868.
[6] B. Polagye, P. Malte, M. Kawase, D. Durran, Effect of large-scale kinetic power extraction on time-dependent estuaries, Proc. Inst. Mech. Eng. Part A J. Power Energy 222 (2008) 471–484.
[7] Deltares, Delft3D: Hydro-morphodynamics, Delft3D, Delft, The Netherlands, 2014, 712 pp.
[8] S. Baston, S. Waldman, J. Side, Modelling Energy Extraction in Tidal Flows, Revision 3.1, Edinburgh, UK, 2014, 39 pp.
[9] S. Mungar, Hydrodynamics of Horizontal-axis Tidal Current Turbines, Technical University of Delft, Delft, The Netherlands, 2014, 157 pp.
[10] Y. Chen, B. Lin, J. Lin, Modelling tidal current energy extraction in large area using a three-dimensional estuary model, Comput. Geosci. 72 (2014) 76–83.
[11] S.P. Neill, E.J. Litt, S.J. Couch, A.G. Davies, The impact of tidal stream turbines on large-scale sediment dynamics, Renew. Energy 34 (2009) 2803–2812.
[12] L. Amoudry, P.S. Bell, K.S. Black, R.W. Gatliff, R. Helsby, A.J. Souza, P.D. Thorne, J. Wolf, A Scoping Study on: Research into Changes in Sediment Dynamics Linked to Marine Renewable Energy Installations, Edinburgh, UK, 2009, 101 pp.
[13] S.P. Neill, J.R. Jordan, S.J. Couch, Impact of tidal energy converter (TEC) arrays on the dynamics of headland sand banks, Renew. Energy 37 (2012) 387–397.
[14] P.E. Robins, Influence of tidal energy extraction on fine sediment dynamics, Oxford, UK, in: R.H.J. Willden, T. Nishino (Eds.), 2nd Oxford Tidal Energy Workshop, Oxford, UK, 2013, pp. 27–28.
[15] R. Ahmadian, R. Falconer, B. Bockelmann-Evans, Far-field modelling of the hydro-environmental impact of tidal stream turbines, Renew. Energy 38 (2012) 107–116.
[16] DOE, Report to Congress on the Potential Environmental Effects of Marine and Hydrokinetic Energy Technologies, GO-102009-2955, Washington, DC, 2009, 143 pp.
[17] H. Bailey, B. Senior, D. Simmons, J. Rusin, G. Picken, P.M. Thompson, Assessing underwater noise levels during pile-driving at an offshore windfarm and its potential effects on marine mammals, Mar. Pollut. Bull. 60 (2010) 888–897.
[18] CMACS, A Baseline Assessment of Electromagnetic Field Generated by Offshore Windfarm Cables, COWRIE Report EMF - 01-2002 66, Liverpool, UK, 2003, 71 pp.
[19] T. Tricas, A. Gill, Effects of EMFs from Undersea Power Cables on Elasmobranchs and Other Marine Species, BOEMRE 2011-09, Camarillo, CA, 2011, 426 pp.
[20] B. Polagye, J. Joslin, A. Stewart, A. Copping, Integrated instrumentation for marine energy monitoring, in: 2nd International Conference on Environmental Interactions of Marine Renewable Energy Technologies, EIMR, Stornoway, Scotland, 2014, pp. 1–3.
[21] J.M. Hamrick, The Environmental Fluid Dynamics Code: User Manual, EFDC User Manual: Version 1.01, Fairfax, VA, 2007, 231 pp.
[22] J.M. Hamrick, The Environmental Fluid Dynamics Code: Theory and Computation, EFDC Theory and Computation: Version 1.01, Fairfax, VA, 2007, 60 pp.
[23] S.C. James, Sandia National Laboratories Environmental Fluid Dynamics Code: Marine Hydrokinetic Module User's Manual, SAND2014-1804, Albuquerque, NM, 2014, 33 pp.
[24] G.G. Katul, L. Mahrt, D. Poggi, C. Sanz, One- and two-equation models for canopy turbulence, Bound. Layer Meteorol. 113 (2004) 81–109.
[25] P.-E. Réthoré, N.N. Sørensen, F. Zahle, Study of the atmospheric wake turbulence of a CFD actuator disc model, Marseille, France, in: European Wind Energy Convention, 2009, pp. 1–9.
[26] C.F. Cerco, T. Cole, User's Guide to the CE-qual-icm Three-dimensional Eutrophication Model, Release Version 1.0, Technical Report EL-95-15, 1995, 316 pp.
[27] K. Park, A.Y. Kuo, J. Shen, J.M. Hamrick, A Three-dimensional Hydrodynamic-eutrophication Model (HEM-3D): Description of Water Quality and Sediment Process Submodels, Special Report in Applied Marine Science and Ocean Engineering No. 327, Gloucester Point, VA, 1995, 204 pp.
[28] S.C. James, C.A. Jones, M.D. Grace, J.D. Roberts, Advances in sediment transport modelling, J. Hydraul. Res. 48 (2010) 754–763.
[29] C.A. Jones, A Sediment Transport Model, University of California Santa Barbara, Santa Barbara, CA, 2001, 119 pp.
[30] F. O'Donncha, S.C. James, N. O'Brien, E. Ragnoli, Parallelisation of a hydro-environmental model for simulating marine current devices, in: MTS/IEEE *OCEANS'15* Conference, Washington, DC, 2015, pp. 1–7.
[31] F. O'Donncha, E. Ragnoli, F. Suits, Parallelisation study of a three-dimensional environmental flow model, Comput. Geosci. 64 (2014) 96–103.
[32] G.L. Mellor, T. Yamada, Development of a turbulence closure model for geophysical fluid problems, Rev. Geophys. 20 (1982) 851–875.
[33] B. Galperin, L.H. Kantha, S. Hassid, A. Rosati, A quasi-equilibrium turbulent energy model for geophysical flows, J. Atmos. Sci. 45 (1988) 55–62.
[34] A.F. Blumberg, G.L. Mellor, A description of a three-dimensional coastal ocean circulation model, in: N.S. Heaps (Ed.), Three Dimensional Coastal Ocean Models Conference, American Geophysical Union, Washington, DC, 1987, pp. 1–16.
[35] S. Peng, G.Y.Z. Fu, X.H. Zhao, B.C. Moore, Integration of environmental fluid dynamics code (EFDC) model with Geographical Information System (GIS) platform and its applications, J. Environ. Inf. 17 (2011) 75–82.
[36] B.J. Tuckey, M.T. Gibbs, B.R. Knight, P.A. Gillespie, Tidal circulation in Tasman and Golden Bays: Implications for river plume behaviour, New Zeal. J. Mar. Freshwat. Res. 40 (2006) 305–324.
[37] Z.-G. Ji, Hydrodynamics, Water Quality, Modeling Rivers, Lakes, and Estuaries, John Wiley and Sons, Hoboken, NJ, 2008.
[38] Z.G. Ji, M.R. Morton, J.M. Hamrick, Wetting and drying simulation of estuarine processes, Estuar. Coast. Shelf Sci. 53 (2001) 683–700.
[39] S.C. James, P.L. Shrestha, J.D. Roberts, Modeling noncohesive sediment transport using multiple sediment size classes, J. Coast. Res. 22 (2006) 1125–1132.
[40] S.C. James, V. Janardhanam, D.T. Hanson, Simulating pH effects in an algal-growth hydrodynamics model, J. Phycol. 49 (2013) 608–615.
[41] S.C. James, J. Barco, E. Johnson, J.D. Roberts, S. Lefantzi, Verifying marine-hydro-kinetic energy generation simulations using SNL-EFDC, in: MTS/IEEE *OCEANS'11* Conference, Kona, HI, 2011, pp. 1–9.
[42] S.C. James, E. Seetho, C. Jones, J. Roberts, Simulating environmental changes due to marine hydrokinetic energy installations, in: MTS/IEEE OCEANS'10 Conference, Seattle, WA, 2010, pp. 1–10.
[43] X. Yang, A. Khosronejad, S. Chawdhary, A. Calderer, D. Angelidis, L. Shen, F. Sotiropoulos, Simulation-based approach for site-specific optimization of marine and hydrokinetic energy conversion systems, in: 36th IAHR World Congress, Spain Water and IWHR, The Hague, The Netherlands, 2015, pp. 1–4.
[44] S. Kang, I. Borazjani, J.A. Colby, F. Sotiropoulos, Numerical simulation of 3D flow past a real-life marine hydrokinetic turbine, Adv. Water Resour. 39 (2012) 33–43.
[45] F. Sotiropoulos, S. Kang, X. Yang, Large-eddy simulation of turbulent flow past hydrokinetic turbine arrays in natural waterways, in: American Geophysical Union Fall Meeting, San Francisco, CA, 2012.
[46] N. Barltrop, K.S. Varyani, A. Grant, D. Clelland, X.P. Pham, INvestigation into wave–current interactions in marine current turbines, Proc. Inst. Mech. Eng. Part A J. Power Energy 221 (2007) 233–242.
[47] P. Galloway, L. Myers, A. Bahaj, Studies of a scale tidal turbine in close proximity to waves, in: 3rd International Conference on Ocean Energy, Bilbao, Spain, 2010, pp. 1–6.
[48] D. Poggi, A. Porporato, L. Ridolfi, J.D. Albertson, G.G. Katul, The effect of vegetation density on canopy sublayer turbulence, Bound. Layer Meteorol. 111 (2004) 565–587.
[49] P.-E. Réthoré, Wind Turbine Wake in Atmospheric Turbulence, Aalborg University, Aalbork, Denmark, 2009, 187 pp.
[50] W.M.J. Batten, M.E. Harrison, A.S. Bahaj, Accuracy of the actuator disc-RANS approach for predicting the performance and wake of tidal turbines, Phil. Trans. R. Soc. A Math. Phys. Eng. Sci. 371 (2013) 1–14.
[51] J.C. Warner, C.R. Sherwood, H.G. Arango, R.P. Signell, Performance of four turbulence closure models implemented using a generic length scale method, Ocean Model. 8 (2005) 81–113.
[52] J. Smagorinsky, General circulation experiments with primitive equations 1: The basic experiment, Mon. Weather Rev. 91 (1963) 99–164.
[53] T. Roc, D.C. Conley, D. Greaves, Methodology for tidal turbine representation in ocean circulation model, Renew. Energy 51 (2013) 448–464.
[54] Z. Yang, T. Wang, A.E. Copping, Modeling tidal stream energy extraction and its effects on transport processes in a tidal channel and bay system using a three-dimensional coastal ocean model, Renew. Energy 50 (2013) 605–613.
[55] C. Chen, G. Cowles, R.C. Beardsley, An Unstructured Grid, Finite-volume Coastal Ocean Model: FVCOM User Manual, Technical Report-04-0601, 2004, 183 pp.

Please cite this article in press as: S.C. James, et al., Simulating current-energy converters: SNL-EFDC model development, verification, and parameter estimation, Renewable Energy (2017), http://dx.doi.org/10.1016/j.renene.2017.07.020

[56] L.E. Myers, A.S. Bahaj, Experimental analysis of the flow field around horizontal axis tidal turbines by use of scale mesh disk rotor simulators, Ocean Eng. 37 (2010) 218–227.
[57] J.I. Whelan, J.M.R. Graham, J. Peiró, A free-surface and blockage correction for tidal turbines, J. Fluid Mech. 624 (2009) 281–291.
[58] L.E. Myers, A.S. Bahaj, Near wake properties of horizontal axis marine current turbines, in: 8th European Wave and Tidal Energy Conference, Uppsala, Sweden, 2009, pp. 558–565.
[59] V.S. Neary, B. Gunawan, C. Hill, L.P. Chamorro, Wake Flow Recovery Downstream of a 1:10 Scale Axial Flow Hydrokinetic Turbine Measured with Pulse-coherent Acoustic Doppler Profiler (PC-ADP), ORNL/TML-2012, 2012, 12 pp.
[60] P.J. Roache, Perspective: a method for uniform reporting of grid refinement studies, J. Fluids Eng. 116 (1994) 405–413.
[61] L.E. Myers, A.S. Bahaj, R.I. Rawlinson-Smith, M. Thomson, The effect of boundary proximity upon the wake structures of horizontal axis marine current turbines, in: 27th International Conference on Offshore Mechanics and Artic Engineering, ASME, Estoril, Portugal, 2008, pp. 709–719.
[62] M.E. Harrison, W.M.J. Batten, L.E. Myers, A.S. Bahaj, A comparison between CFD simulations and experiments for predicting the far wake of horizontal axis tidal turbines, in: 8th European Wave and Tidal Energy Conference, Uppsala, Sweden, 2009, pp. 566–575.
[63] L. Myers, A.S. Bahaj, Near wake properties of horizontal axis marine current turbines, in: 8th European Wave and Tidal Energy Conference, Uppsala, Sweden, 2009, pp. 558–565.
[64] W.M.J. Batten, M.E. Harrison, A.S. Bahaj, Accuracy of the actuator disc-RANS approach for predicting the performance and wake of tidal turbines, Phil. Trans. R. Soc. A 371 (2013) 20120293.
[65] V.S. Neary, B. Gunawan, C. Hill, L.P. Chamorro, Near and far field flow disturbances induced by model hydrokinetic turbine: ADV and ADP comparison, Renew. Energy 60 (2013) 1–6.
[66] A.-B.S. Bahaj, L.E. Myers, M.D. Thomson, N. Jorge, Characterising the wake of a horizontal axis marine turbine, in: 7th European Wave and Tidal Energy Conference, Porto, Portugal, 2007, pp. 1–9.
[67] J.E. Doherty, Model-independent Parameter Estimation User Manual Part II: PEST Utility Support Software, PEST Addendum, Brisbane, Australia, 2016, 226, pp.
[68] J.E. Doherty, Model-independent Parameter Estimation User Manual Part I: PEST, SENSAN and Global Optimisers, PEST Manual, Brisbane, Australia, 2016, 390, pp.
[69] S.C. James, J.E. Doherty, A.-A. Eddebbarh, Practical postcalibration uncertainty analysis: Yucca Mountain, Nevada, Ground Water 47 (2009) 851–869.
[70] T. Stallard, R. Collings, T. Feng, J. Whelan, Interactions between tidal turbine wakes: experimental study of a group of three-bladed rotors, Phil. Trans. R. Soc. A 371 (2013) 20120159.
[71] K. Nelson, S.C. James, J.D. Roberts, C.A. Jones, A framework for determining improved placement of current energy converters subject to environmental constraints, Int. J. Sustain. Energy (2017) 1–15. http://www.tandfonline.com/doi/abs/10.1080/14786451.2017.1334654?journalCode=gsol20.
[72] F. O'Donncha, E. Ragnoli, S. Venugopal, S.C. James, K. Katrinis, On the efficiency of executing hydro-environmental models on Cloud, Procedia Eng. 154 (2016) 199–206.
[73] B. Gunawan, V.S. Neary, S. Grovue, J. Mortensen, B. Heiner, Field measurement test plan to determine effects of hydrokinetic turbine deployment on canal test site in Yakima, WA, USA, in: 2nd Marine Energy Technology Symposium, METS2014, Seattle, WA, 2014, pp. 1–8.
[74] B. Gunawan, J. Roberts, V.S. Neary, Hydrodynamic effects of hydrokinetic turbine deployment in an irrigation canal, in: 3rd Marine Energy Technology Symposium, METS2015, Washington, DC, 2015.
[75] J.E. Doherty, D.E. Welter, A short exploration of structural noise, Water Resour. Res. 46 (2010). W05525.
[76] T. Blackmore, W.M.J. Batten, A.S. Bahaj, Influence of turbulence on the wake of a marine current turbine simulator, Proc. R. Soc. A Math. Phys. Eng. Sci. 470 (2014), 20140331.
[77] P.M. Craig, User's Manual for EFDC_Explorer: A Pre/Post Processor for the Environmental Fluid Dynamics Code, EFDC_Explorer, 2016, 2016, 391 pp.

Please cite this article in press as: S.C. James, et al., Simulating current-energy converters: SNL-EFDC model development, verification, and parameter estimation, Renewable Energy (2017), http://dx.doi.org/10.1016/j.renene.2017.07.020